ACS APPLIED MATERIALS & INTERFACES

Research Article

Cite This: ACS Appl. Mater. Interfaces XXXX, XXX, XXX−XXX

www.acsami.org

Tumor Homing Reactive Oxygen Species Nanoparticle for Enhanced Cancer Therapy

Hyeon-Yeol Cho,[†,‡,○] Ahmet Mavi,[§,○] Sy-Tsong Dean Chueng,[†] Thanapat Pongkulapa,[†] Nicholas Pasquale,[†] Hudifah Rabie,[†] Jiyou Han,[∥] Jong Hoon Kim,[⊥] Tae-Hyung Kim,[*,#] Jeong-Woo Choi,[*,‡] and Ki-Bum Lee[*,†,▽]

[†]Department of Chemistry and Chemical Biology, Rutgers, The State University of New Jersey, Piscataway, New Jersey 08854, United States

[‡]Department of Chemical & Biomolecular Engineering, Sogang University, Seoul 04107, Republic of Korea

[§]Department of Nanobiotechnology, Atatürk University, Erzurum 25030, Turkey

[∥]Department of Biological Sciences, Laboratory of Stem Cell Research and Biotechnology, Hyupsung University, Hwasung-si 18330, Republic of Korea

[⊥]Department of Biotechnology, Laboratory of Stem Cells and Tissue Regeneration, College of Life Sciences and Biotechnology, Korea University, Seoul 02841, Republic of Korea

[#]School of Integrative Engineering, Chung-Ang University, Seoul 06974, Republic of Korea

[▽]Department of Life and Nanopharmaceutical Science, College of Pharmacy, Kyung Hee University, Seoul 02447, Republic of Korea

Supporting Information

ABSTRACT: Multifunctional nanoparticles that carry chemotherapeutic agents can be innovative anticancer therapeutic options owing to their tumor-targeting ability and high drug-loading capacity. However, the nonspecific release of toxic DNA-intercalating anticancer drugs from the nanoparticles has significant side effects on healthy cells surrounding the tumors. Herein, we report a tumor homing reactive oxygen species nanoparticle (THoR-NP) platform that is highly effective and selective for ablating malignant tumors. Sodium nitroprusside (SNP) and diethyldithiocarbamate (DDC) were selected as an exogenous reactive oxygen species (ROS) generator and a superoxide dismutase 1 inhibitor, respectively. DDC-loaded THoR-NP, in combination with SNP treatment, eliminated multiple cancer cell lines effectively by the generation of peroxynitrite in the cells (>95% cell death), as compared to control drug treatments of the same concentration of DDC or SNP alone (0% cell death). Moreover, the magnetic core ($ZnFe_2O_4$) of the THoR-NP can specifically ablate tumor cells (breast cancer cells) via magnetic hyperthermia, in conjunction with DDC, even in the absence of any exogenous RS supplements. Finally, by incorporating iRGD peptide moieties in the THoR-NP, integrin-enriched cancer cells (malignant tumors, MDA-MB-231) were effectively and selectively killed, as opposed to nonmetastatic tumors (MCF-7), as confirmed in a mouse xenograft model. Hence, our strategy of using nanoparticles embedded with ROS-scavenger-inhibitor with an exogenous ROS supplement is highly selective and effective cancer therapy.

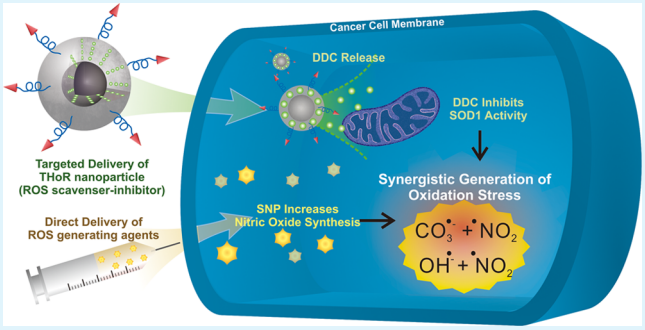

KEYWORDS: *nanotechnology, magnetic core−shell nanoparticles, cancer therapy, reactive species, tumor targeting*

INTRODUCTION

Nanoparticle-based cancer therapies have emerged as a new promising approach owing to the excellent physicochemical properties of nanoparticles, which allow conjugation of cancer-targeting moieties,[1,2] high drug-loading capacity,[3−5] and active function through external forces (e.g., magnetic and photothermal hyperthermia).[6−8] Conventional nanoparticle-based cancer therapies use nanomaterials as a drug carrier to block DNA replication and transcription, resulting in the apoptosis of target cancer cells. However, such therapies still suffer from drug leakage issue in the physiological condition, mostly due to the substitution reaction of biomolecules and ions. Therefore, undesirable adverse effects to the surrounding healthy tissues and organs are unavoidable, which lead to vomiting, nausea, low blood count, and diarrhea in patients undergoing chemotherapies.[9−11]

Received: April 30, 2019
Accepted: June 11, 2019

DOI: 10.1021/acsami.9b07483
ACS Appl. Mater. Interfaces XXXX, XXX, XXX−XXX

Reactive oxygen species (ROS) are highly reactive molecules produced by mitochondria in aerobic cells during its energy production.[12−14] A moderate level of ROS is nontoxic and can enhance cellular functions, such as proliferation, migration, and differentiation,[15] whereas high levels of ROS cause oxidative stress/damage to cellular components (e.g., lipids, enzymes, proteins, and DNAs/RNAs), resulting in cell death.[14] Thus, to maintain proper levels of ROS, cells regulate their intracellular ROS levels via ROS-scavengers: superoxide dismutases (SOD1, SOD2, and SOD3), glutathione peroxidase, glutaredoxin, and catalase.[16−18] Due to the destructive nature of ROS, elevated ROS levels have also been considered as an attractive strategy for cancer tumor treatment by direct delivery of ROS-generating agents and ROS-scavenger-inhibitors in the abnormal/cancer cells to induce cell apoptosis.[19−21] In particular, motexafin gadolinium (gadolinium texaphyrin) and β-lapachone (ARQ 501) are representative exogenous ROS-generating agents, which have been under clinical trials for cancer treatment.[22,23] Other small molecule drugs, such as buthionine sulfoximine,[24] imexon,[25] and 2-methoxyestradiol,[26] have also been intensively studied as anticancer agents, acting mainly via antioxidant inhibition, including glutathione and SOD. However, these ROS-modulating drug candidates are not free from the adverse effects associated with drug toxicity. Therefore, the development of a targeted tumor cell ablation strategy without damaging neighboring healthy cells is essential.

One of the most attractive features of ROS-mediated cancer treatment approach is that ROS only induce cell apoptosis at high intracellular concentrations.[27−29] Thus, selectively increasing ROS levels in the target cells by delivering both ROS-releasing molecules and ROS-scavenger-inhibitors is a more viable option for treating cancers, as compared to the expensive and time-consuming process of developing new cancer-specific drugs.[30−34] Considering the advantages of drug-loaded nanoparticles in cancer targeting, loading a single ROS-triggering factor is highly effective for target-specific cancer ablation. Therefore, a simple single drug-loading system is better than complex nanoparticles loaded with multiple drugs or complex functionalities, as it is easy to synthesize, standardize, and is effective at inducing cancer cell apoptosis when combined with exogenous ROS-releasing drugs (ROS supplements) through conventional methods such as subcutaneous injection and oral administration. Moreover, the excess ROS introduced via supplements can be eliminated efficiently by antioxidant administration, as opposed to DNA-intercalating chemotherapeutic agents (e.g., doxorubicin, camptothecin), which damage normal/healthy cells permanently.[35,36]

Thus, we report a new strategy with tumor homing ROS nanoparticles (THoR-NPs) utilizing an ROS-generating agent (sodium nitroprusside, SNP) and an ROS-scavenger-inhibitor (diethyldithiocarbamate, DDC) via iRGD-conjugated magnetic core−shell silica nanoparticles to selectively ablate two types of malignant tumors (glioblastoma and breast cancer) (Figure 1). As highly elevated levels of ROS are not toxic to cells in the presence of ROS-scavengers, we have designed a simple system, for the first time, which uses nanoparticles to deliver a ROS-scavenger-inhibitor to malignant tumor cells (integrin over-expressing cells), whereas ROS-generating molecules are freely delivered to cells without using targeting moieties. SNP is a well-known nitric oxide-releasing molecule, and DDC is a strong SOD1 inhibitor.[37−40] Hence, due to the synergistic effects of SNP and DDC on cancer cells, only cells exposed to both SNP and DDC-loaded nanoparticles showed a highly elevated level of ROS, resulting in significant cell death via ROS-mediated apoptosis. Moreover, we have also confirmed that specific tumors, such as breast cancer (MDA-MB-231), were effectively sensitized via magnetic field-mediated ROS generation. Finally, by integrating an iRGD ligand for the selective delivery of DDC into tumors expressing high levels of integrin (MDA-MB-231),[41−43] we have confirmed that malignant tumors can be selectively ablated using our THoR-NP platform in conjunction with free SNP treatment for in vitro and in vivo conditions.

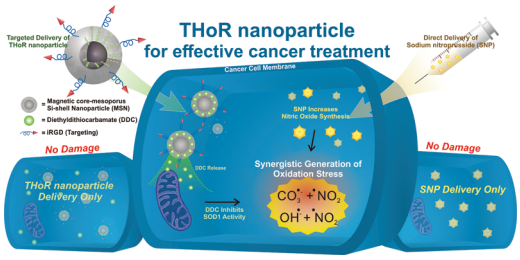

Figure 1. Tumor homing reactive nanoparticle (THoR-NP) platform was created to avoid damage to neighboring healthy cells in a reactive oxygen species (ROS)-based cancer therapy. THoR-NP comprises a magnetic core, mesoporous silica shell, and iRGD peptide and can specifically deliver ROS-scavenger inhibitor diethyldithiocarbamate (DDC) into targeted cancer cells. Working synergistically with locally generated ROS and exogenously ROS-generating agents, sodium nitroprusside (SNP) and DDC, delivered to the cytosol of cancer cells through THoR-NP, directly damage organelles, disrupt cancer growth, and lead to tumor ablation. Individual treatments of THoR-NP′ or ROS-generating reagent do not show any anticancer or adverse effects to minimize off-target cell death.

RESULTS AND DISCUSSION

ROS-Mediated Cell Apoptosis Strategy using DDC-Loaded Mesoporous Silica Nanoparticles. ROS levels in cancer cells must be significantly increased to induce cell apoptosis. Aerobic cells naturally produce various ROS, such as superoxide radical ($O_2^{\bullet-}$), hydrogen peroxide (H_2O_2), hydroxyl radical ($OH^{\bullet}$), and hypochlorous acid (HOCl), and RNS, such as nitric oxide ($NO^{\bullet}$) and peroxynitrite ($ONOO^-$).[44,45] As ROS are toxic metabolic products, cells activate various antioxidant enzymes to balance the ROS levels.[16] Imbalance in ROS generation/elimination induces oxidative stress, and the increase in the ROS concentration leads to undesirable changes in molecular functions of cells due to oxidation of essential biomolecules. Hence, one of the most effective ways to increase intracellular ROS levels is to inhibit antioxidant enzymes.[17] Considering that 1−4% of the mitochondrial oxygen consumption is incompletely reduced to $O_2^{\bullet-}$ to yield H_2O_2, $OH^{\bullet}$, HOCl, and $ONOO^-$ via various enzymatic or nonenzymatic reactions, we hypothesized that SODs (CuZnSOD, MnSOD, and ECSOD), which catalyze the dismutation of $O_2^{\bullet-}$ into O_2 and H_2O_2, are the most important antioxidant enzymes involved in the ROS-scavenging system.[44−48] The inhibition of SOD enzymes disturbs the $O_2^{\bullet-}$ detoxification pathway, ultimately resulting in the accumulation of $O_2^{\bullet-}$ in cytoplasm and mitochondria.

$ONOO^-$ is the most destructive derivative of $O_2^{\bullet-}$ and is typically generated by a reaction between $O_2^{\bullet-}$ and $NO^{\bullet}$. Both $NO^{\bullet}$ and $ONOO^-$ are highly reactive molecules. However, $ONOO^-$ interacts with biomolecules more actively with a

DOI: 10.1021/acsami.9b07483
ACS Appl. Mater. Interfaces XXXX, XXX, XXX−XXX

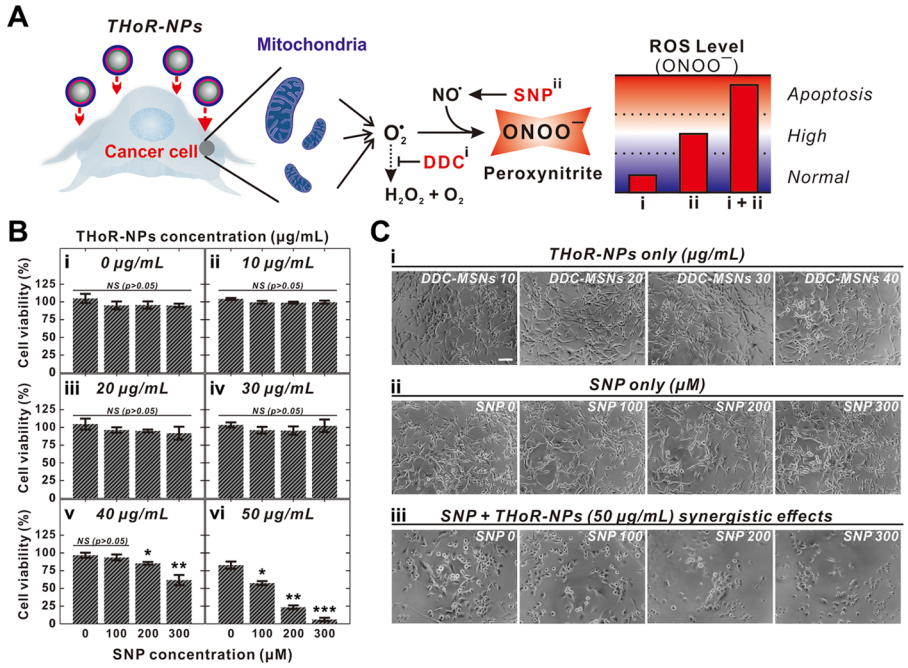

Figure 2. Synergistic effects of SNP and DDC on glioblastoma. (A) Schematic diagram of an intracellular ROS generation mechanism after DDC-NP and SNP delivery into a cancer cell. To effectively increase the amount of destructive ROS molecule, $ONOO^-$ in this case, the ROS-scavenging activity of SOD1 should be silenced prior to $NO^•$ supplement via SNP treatment. (B) Dose-dependent synergistic anticancer effects with DDC-loaded THoR-NP and SNP on glioblastoma were determined using the 3-(4,5-dimethylthiazol-2-yl)-5-(3-carboxymethoxyphenyl)-2-(4-sulfophenyl)-2*H*-tetrazolium (MTS) assay. DDC-NPs were treated at 0, 10, 20, 30, and 40 μg/mL and SNP was treated at 0, 100, 200, and 300 μM. Less than 10% of the cells survived the THoR-NP treatment (50 μg/mL) and SNPs treatment (300 μM). (C) Phage image of glioblastoma after the combined treatment of THoR-NP and SNPs. The data represent means ± standard deviations (SD) of five different experiments ($*p < 0.05$, $**p < 0.01$, $***p < 0.0001$).

short half-life (10−20 ms) while generating additional destructive ROS, such as $CO_3^{•-}$, $NO_2^•$, and $OH^•$.[49] Thus, DDC, a CuZnSOD inhibitor, was used to block the pathway responsible for converting $O_2^{•-}$ to H_2O_2 and O_2, and SNP was used as an exogenous $NO^•$ source to facilitate the generation of $ONOO^-$ (Figure S1A).[37,39] Increased intracellular levels of $NO^•$ are controlled by ROS-scavengers. Therefore, we designed a nanoparticle platform loaded with SOD1 inhibitor (DDC) and conjugated integrin-targeting ligands onto the nanoparticle surface to selectively sensitize aggressive tumors (integrin over-expressing cells). This strategy enabled exposing only cells with DDC-loaded THoR-NPs to an uncontrollable amount of ROS, leading to cell apoptosis via both SOD1 inhibition and exogenously delivered ROS-releasing molecules. THoR-NPs were designed to have a diameter of 60 nm and a surface charge of +30 mV (Figure S2) to facilitate the uptake of nanoparticles and to absorb more DDC molecules in mesoporous silica shell via electrostatic interactions (loading efficiency = 15.21%, entrapment efficiency = 13.69%).[50] In terms of drug release capability, 51.73% of DDC was found to be released from the nanoparticles after 60 h of incubation in phosphate buffer saline (pH 7.4), due in part to the positively charged surface of THoR-NPs that allows for the sustained release of DDC (Figure S3). In addition, the magnetic core of the THoR-NP was utilized to effectively generate ROS on exposing to an alternating magnetic field, which could ablate cancer cells without using toxic exogenous ROS. Combining the integrin-targeting iRGD moieties allowed us to target malignant tumors such as brain (U87-EGFR-viii) and breast cancer cells (MDA-MB-231) using DDC-loaded THoR-NPs for SOD1 inhibition, whereas ROS generation was facilitated by exogenous molecule (SNP) and magnetic hyperthermia (Figure S1B).

Synergistic Effects of SNP and DDC on Glioblastoma and Breast Cancer Cell Apoptosis. ROS are naturally produced from the mitochondrial energy production cycles and are toxic to cells when their concentration is higher than the threshold (uncontrollable state).[14,16] Thus, to investigate the optimal concentration of ROS supplements and ROS-inhibiting molecules for selective chemotherapy, their synergistic effects were confirmed by varying the concentration of each component. This evaluation was critical in determining the optimal treatment conditions for selective cancer cell ablation with minimum damage to the neighboring healthy cells.

To effectively increase the concentration of destructive ROS molecule, $ONOO^-$ in this case, the ROS-scavenging activity of SOD1 was disabled via SNP treatment, prior to $NO^•$ supplementation (Figure 2A).[51] THoR-NPs were, thus, first delivered to two different types of malignant tumors, glioblastoma (U87-EGFR-viii) and breast cancer (MDA-MB-231), followed by SNP treatment to significantly increase the ROS levels in intracellular environments (Figures 2B,C and S4). When administrated alone, both SNP and DDC-loaded THoR-NPs showed no toxicity on glioblastoma within the concentration ranges of 0−300 μM and 0−30 μg/mL, respectively, which was consistent with our hypotheses. However, when administrated simultaneously, cell viability decreased significantly, especially at high doses of DDC-loaded THoR-NPs. At a THoR-NP concentration of 40 μg/mL, SNP was found to affect cell viability at concentrations higher than 200 μM. Synergistic effects of both THoR-NPs and SNP were

DOI: 10.1021/acsami.9b07483
ACS Appl. Mater. Interfaces XXXX, XXX, XXX−XXX

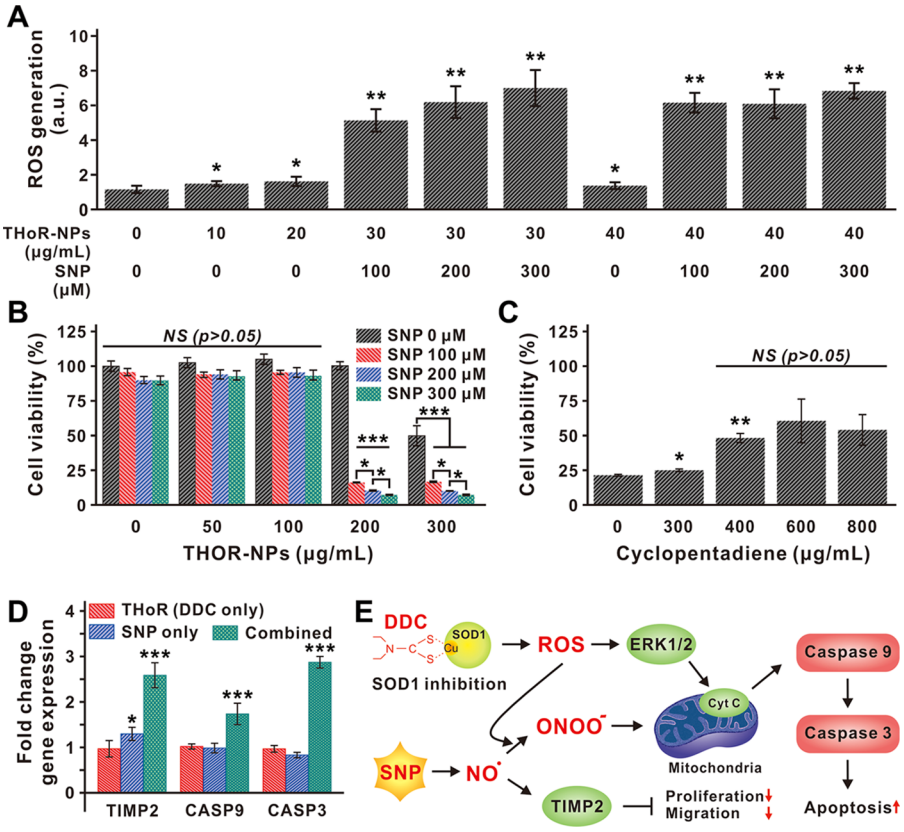

Figure 3. Confirmation of generation of reactive species and its anticancer effects on glioblastoma. (A) Dose-dependent synergistic ROS generation with THoR-NP and SNP treatment was measured based on fluorescence signal of ROS reactive reagent 2′,7′-dichlorofluorescin diacetate (DCFH-DA) (100 μM). THoR-NP was treated at concentrations of 0, 10, 20, 30, and 40 μg/mL, and SNP was treated at concentrations of 0, 100, 200, 300 μM. (B) The ROS inhibition analysis with antioxidant (2 mM, *N*-acetylcysteine) treatment was carried out to confirm the anticancer effects of generated ROS from DDC-NP and SNP on U87-EGFR-viii. Less than 10% of the cells survived under THoR-NP (100 μg/mL) and SNPs (300 μM) treatment condition. (C) The effects of cyclopentadiene, the $ONOO^-$ scavenger, were measured to validate the generation of $ONOO^-$ at fixed concentrations of SNP and DDC. The cell viability increased upon cyclopentadiene treatment up to a concentration of 400 μM. (D) Quantitative reverse transcription PCR (RT-qPCR) showed synergistic upregulation of ROS-related genes, including cancer growth (TIMP2) and apoptosis (caspase 9 [CASP9], caspase 3 [CASP3]). (E) Schematic diagram depicting the proposed mechanism that synergistically generates $ONOO^-$ with SNP and DDC co-treatment. The data represent means ± SD of five different experiments (*p < 0.05, **p < 0.01, ***p < 0.001).

apparent at 50 μg/mL and 300 μM, respectively, which eliminated more than 95% of glioblastoma. The same concentration of SNP was not toxic in the same cell line at 30 μg/mL of THoR-NPs, proving a clear synergistic effect of SNP and DDC on ROS-mediated cell apoptosis. Interestingly, owing to variations in the intracellular environments concerning ROS production and ROS-scavenging systems, breast cancer cells were more sensitive to SNP and DDC treatment at a lower concentration of DDC (30 μg/mL). Thus, the demonstrated strategy of using DDC as a SOD1 inhibitor and SNP as ROS supplement to generate destructive $ONOO^-$ molecule was highly effective for ablation of two different types of malignant tumors.

Confirmation of ROS Generation and Effects of Antioxidants on Cell Death. As DDC was used as a SOD1 inhibitor for cancer ablation, we next sought to investigate whether cells were affected by the increased amount of ROS or the toxicity of DDC itself. DDC, a metabolite of disulfiram, is a water-soluble, potent, copper-chelating compound, which is capable of inhibiting the CuZnSOD enzyme.[39] However, DDC can also react with various intracellular proteins and is known to be cytotoxic.[52] The toxicity of DDC can be attributed to several different mechanisms: inhibition of DNA methyltransferase, reduction of NF-kB activation, reduction of DNA replication, and inhibition of interleukin-1 converting enzyme (ICE-1).[39,40] Hence, to investigate the increase in the ROS levels in response to SNP and DDC treatments, we confirmed ROS generation by varying the SNP and DDC concentrations.

Consistent with our expectations, both DDC and SNP were found to increase ROS levels in the cells, whereas DDC alone was less effective as compared to the SNP treatment (Figure 3A). Interestingly, the ROS levels were around 5−7 fold higher than the control group (no DDC and SNP treatment) when both DDC-loaded THoR-NPs and SNP were delivered, indicating that the cell apoptosis (confirmed in Figure 2) was contributed to the synergistic effect of SNP and DDC on ROS generation. Comparing with previously reported ROS-generating agents or ROS-scavenger-inhibitors, the DDC-loaded THoR-NPs alone showed similar ROS-generating efficiency (1.85 folds, literature: 2.1 folds,[22] 2.3 folds,[23] and 2.1 folds[24]). However, ROS generation induced by DDC-loaded THoR-NPs was slightly lower than the numbers reported by the previous literature, which might be due to the self-limiting effect that was regulated by the upregulation of several antioxidant response element-mediated genes such as Nrf1 and Nrf2.[53] To further investigate, one of the antioxidants (2 mM, *N*-acetylcysteine), effective for ROS species removal,

DOI: 10.1021/acsami.9b07483
ACS Appl. Mater. Interfaces XXXX, XXX, XXX−XXX

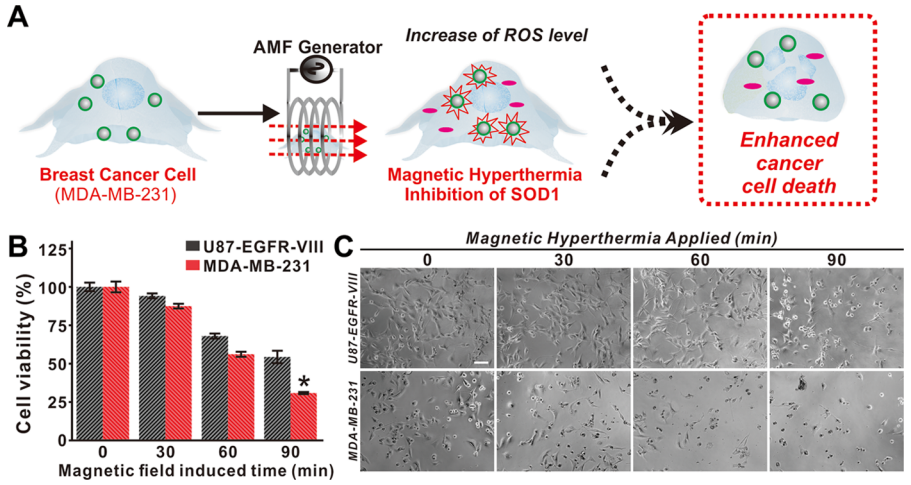

Figure 4. Effects of magnetic hyperthermia using DDC-loaded THoR-NP. (A) Schematic diagram of an application of THoR-NP-induced magnetic hyperthermia. After the uptake, the anticancer effect of intracellular THoR-NP was enhanced with the release of the DDC, SOD1 inhibitor, and generation of heat with an alternating magnetic field (AMF). (B) The anticancer effects of magnetic hyperthermia on cancer cells of different origins with different AMF applying time. (C) The phage images of cancer cells with magnetic hyperthermia. The data represent means ± SD of five different experiments (*$p < 0.05$).

was treated in the presence of both SNP and DDC-loaded THoR-NPs.[54] As shown in Figure 3B, cells showed a low loss in viability at 50 μg/mL DDC-loaded THoR-NPs and 300 μM SNP, in contrast to the results (Figure 2) in the absence of antioxidants. Remarkably, cells showed more than 90% viability even at extremely high concentrations of DDC-loaded THoR-NPs (100 μg/mL) and SNPs (300 μM), confirming that antioxidants protect the cells from ROS-mediated cell death. However, when the concentration of DDC-loaded THoR-NPs delivered was higher than 200 μg/mL, cell viability decreased by more than 90%, owing to the imbalance of antioxidant and ROS generation mediated by DDC and SNP co-treatment. Thereafter, cyclopentadiene, the $ONOO^-$ scavenger, was used to check whether $ONOO^-$, generated by DDC and SNP co-treatment, was involved in cell apoptosis by evaluating cell viability in response to varying concentrations of cyclopentadiene at fixed concentrations of SNP and DDC.[55] As shown in Figure 3C, cell viability recovered up to 70 from 25% in the presence of cyclopentadiene, indicating that apoptosis of cancer cells was triggered by the increase of $ONOO^-$, thus supporting our hypothesis. As cell viability did not recover fully, even at an extremely high concentration of cyclopentadiene (800 μM), further studies are needed to clarify other factors involved in the DDC and SNP cancer co-treatment strategy (Figure S5). To confirm the underlying mechanism of this synergy, we conducted quantitative reverse transcription polymerase chain reaction (RT-qPCR) for DDC and SNP co-treated condition. We found that the co-treatment of DDC and SNP significantly activated the apoptosis-related genes (e.g., caspase 9 and caspase 3) and $NO^•$-related gene (e.g., TIMP2) (Figure 3D) suggesting that only DDC and SNP co-localized cancer cells generated high ROS level, which led to higher levels of apoptosis induction. Moreover, higher expression of TIMP2 with $NO^•$ generation inhibited the proliferation and migration of cancer, which explains the reason why the high concentration of cyclopentadiene was not recovered the cell viability (Figure 3E).

Magnetic Hyperthermia Combined with DDC Treatment for Exogenous ROS-Generating Molecule-Free Treatment. Although the co-treatment strategy using SNP and DDC is quite effective for killing cancer cells at high levels of $ONOO^-$, investigations into cancer cell ablation methods that do not rely on toxic exogenous molecules are worthwhile. Since the THoR-NPs synthesized for this study possessed strong magnetic properties, they could also be used to generate ROS in THoR-NPs-transfected cells via magnetic hyperthermia, useful for cancer treatment in combination with DDC treatment. Reports have shown that hyperthermia decreases the SOD1 mRNA levels, resulting in a decrease of superoxide scavenging activity and an increase in the ROS levels.[55] The alternating magnetic field rotational forces on MNPs in lysosomes were found to not only distribute lysosomes but also enhance lysosomal permeability.[56] The enhancement of lysosomal permeability was highly correlated with ROS generation, which could ultimately affect cell viability.[57] To confirm this theory, two different cell lines, MDA-MB-231 (breast cancer) and U87-EGFR-viii (brain cancer), were used. Interestingly, as shown in Figure 4, breast cancer (MDA-MB-231) was found to be highly sensitive to magnetic hyperthermia treatment, wherein cell viability decreased significantly to ~ 30% after 90 min. However, under the same conditions, glioblastoma (U87-EGFR-viii) was not affected as drastically as the MDA-MB-231 cells, regardless of the duration of magnetic hyperthermia application. The difference in the effects of hyperthermia on different types of cancer cells, in conjunction with DDC treatment, may be attributed to distinct characteristics of the brain. The brain consumes more glucose/oxygen and, therefore, generates higher levels of ROS during adenosine triphosphate synthesis, relative to other organs (20% of total oxygen consumption), making it more resistant to free-radical generation.[58] In addition, the brain also possesses a higher antioxidant capacity, as compared to other organs, making neuronal cells more resistant to ROS generation.[59] Additionally, we confirmed that the ROS levels in cells exposed to magnetic hyperthermia, combined with the DDC treatment, increased with the duration of hyperthermia application, proving that cell apoptosis resulted from elevated levels of ROS (Figure S6). Hence, we concluded that along with exogenous molecules, hyperthermia treatment using

DOI: 10.1021/acsami.9b07483
ACS Appl. Mater. Interfaces XXXX, XXX, XXX−XXX

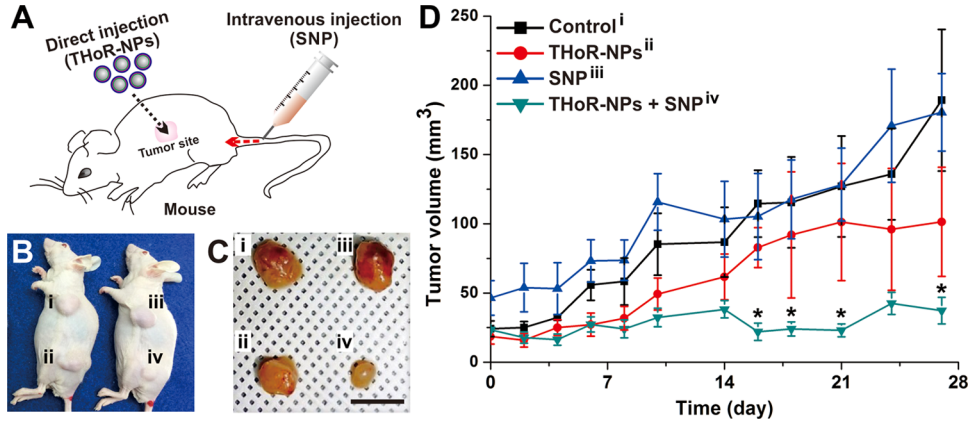

Figure 5. In vivo effects of combined THoR-NPs and SNP therapy. (A) Schematic diagram of THoR-NPs (intratumor injection) and SNP (intravenous injection) delivery into a mouse. THoR-NPs and SNP solutions were injected at an interval of 24 h weekly for 4 weeks. (B) Every mouse had two tumors: one on the left shoulder and one on the left thigh. The mice were separated into two groups based on the SNP treatment condition: group 1, control (phosphate-buffered saline (PBS), i and ii) and group 2, SNP injection (1 mg/kg, iii and iv). In each mouse, THoR-NPs were injected into the tumor on the left thigh, and PBS was injected into the left shoulder as the control group. (C) After 4 weeks, the extracted tumors showed clear size difference in the presence of THoR-NP treated with SNP: (i) PBS/PBS, (ii) THoR-NP/PBS, (iii) PBS/SNP, and (iv) THoR-NP/SNP. Scale bar: 1 mm. (D) Inhibiting the ROS-scavenger with THoR-NPs suppressed the tumor growth. With synergistic administration of SNP, THoR-NP further reduced tumor growth. The size of the tumor was quantified at various time points. Based on the size measurement, the tumor growth was inhibited by synergistic THoR-NP and SNP treatment. (*$p < 0.01$).

magnetic nanoparticles is also a viable option for the treatment of tumors, in combination with a SOD1 inhibitor (DDC).

Target-Specific Delivery and Therapeutic Effects of THoR-NPs. After confirming that using both SNP and DDC for the elevation of intracellular ROS levels promotes cancer cell apoptosis, we next sought to investigate their targeting efficacy toward malignant tumors using integrin-enriched breast cancer as a model cell line (MDA-MB-231) in vitro and in vivo. To achieve this goal, THoR-NPs were functionalized with an iRGD peptide, a proven targeting moiety for targeting the $\alpha v\beta 3$ integrin surface receptors, which are highly expressed in malignant tumors.[43] Two different breast cancer cell lines expressing low (nonmetastatic) and high (malignant) level of integrin, MCF-7, and MDA-MB-231, respectively, were treated with fluorescein isothiocyanate (FITC)-loaded THoR-NPs (50 μg/mL) and analyzed with flow cytometry (Figure S7A). With a higher expression level of integrin, 96.5% population of MDA-MB-231 cells showed significantly high fluorescence intensity, whereas 13.4% of MCF-7 cells showed fluorescence signals. To further confirm the combined therapeutic effects of THoR-NPs and SNP on MCF-7 cells, a higher concentration of THoR-NPs was treated. As shown in Figure S7B, no dramatic decrease in cell viability (50% cell death) was observed in the presence of both THoR-NPs (60 μg/mL) and SNP (300 μM). This observation was entirely different from that in the MDA-MB-231, which showed around 80% cell death at low concentrations (50 μg/mL) of THoR-NPs and SNP (300 μM). When the concentration of THoR-NPs reached 90 μg/mL, 60% cell death was observed, indicating that THoR-NPs were not effectively transfected into low integrin-expressing cells (MCF-7), as opposed to the model malignant tumor (MDA-MB-231). After this, we next developed a mouse tumor xenograft model with the MDA-MB-231 to confirm the biodistribution of THoR-NPs. As shown in Figure S8, the intravenous (iv) injected FITC-loaded THoR-NPs showed time-dependent accumulation on the tumor location specifically in both in vivo and ex vivo imaging, proving excellent in vivo tumor-targeting ability of THoR-NPs. Next, the toxicity of SNP in mice, where SNP was treated via intravenous (iv) injection with different doses, was tested prior to the investigation of therapeutic efficacy of the combined treatment (Table S1). SNP is known to be utilized as an intravenous vasodilator, which has been most clinically used in cardiac surgery,[60] and has been reported to be neurotoxic at concentrations of 2.5 mg/kg or higher, at which lipid peroxidation in brain, kidney, and liver tissue typically occurs. In this study, by varying the concentration of SNP, we found that a concentration of 1 mg/kg or less did not affect survivability at the daily iv injection condition, whereas over 10 mg/kg SNP was found to be toxic 1 h after injection.

After the confirmation of both biodistribution of THoR-NPs and the optimum concentration of SNP for the mouse xenograft model, THoR-NPs and SNP were applied to mice via intratumoral (it) injection (two tumors at the left side of shoulder and flank) and iv injection, respectively, to confirm the synergistic effects of DDC and SNP co-treatment (Figure 5). After 4 weeks of injection, we confirmed that THoR-NPs and SNP co-treatment significantly inhibited the tumor (80% decrease in tumor volume vs control group), whereas THoR-NPs and SNP single treatment showed 47 and 5% decrease in tumor volume, respectively (Figure 5B–D). Moreover, as shown in Figures S9 and S10, no damage to other organs (e.g., liver, kidney, spleen) was observed from both shapes of organs and tissue histology, proving that the THoR-NPs (it injection) and SNP (iv injection) co-treatment was effective for in vivo tumor ablation. In summary, these results suggest that THoR-NP, in combination with an exogenous ROS supplement, is an attractive candidate for targeted cancer therapy with minimal side effects on healthy cells.

CONCLUSIONS

In conclusion, we have shown that our strategy of using nanoparticles containing a ROS-scavenger (SOD1 inhibitor) and an exogenous ROS supplement is excellent for ablating both brain and breast cancer cells, based on ROS-mediated cell apoptosis. Co-treatment of 50 μg/mL THoR-NPs and 300 μM SNP was found to kill more than 95 and 80% glioblastoma

DOI: 10.1021/acsami.9b07483
ACS Appl. Mater. Interfaces XXXX, XXX, XXX−XXX

(U87-EGFR-viii) and breast cancer cells (MDA-MB-231), respectively, whereas DDC or SNP single drug treatment showed no toxicity in either cell line. Using two different types of antioxidants, we further confirmed that cell death occurred mainly due to the high level of ROS, especially $ONOO^-$, contributed by both exogenous ROS supplement (SNP) and SOD1 inhibitor (DDC). The application of the magnetic core of the THoR-NPs also showed that specific cell lines, especially a breast cancer cell line, are vulnerable to ablation via magnetic hyperthermia in conjunction with DDC treatment in toxic exogenous ROS supplement-free conditions. Finally, by incorporating integrin-targeting moieties (iRGD), THoR-NPs were found to selectively ablate integrin-enriched cell lines (MDA-MB-231) over nonmetastatic tumors (MCF-7) in the presence of SNP, indicating that the developed single THoR-NPs are highly effective for tumor-specific cancer therapy causing minimal damage in healthy cells. These in vitro results also matched those from in vivo studies, showing that THoR-NPs therapy, in conjunction with SNP treatment, was effective for tumor growth suppression, whereas SNP or THoR-NPs single treatments failed to show significant inhibition of tumor growth after 4 weeks of evaluation. We have proven that our strategy, involving both the ROS-scavenger inhibitor and the ROS supplement, is effective for selective malignant tumor execution. However, further studies are needed for investigating the optimum drug combinations for ablation of specific types of tumors with minimal damages to normal/healthy cells, based on the tumor-specific ROS elevation method.

METHODS

Reagents. Aminopropyltriethoxysilane (APTES), ammonium nitrate, desferrioxamine, 2′,7′-dichlorofluorescin diacetate (DCFH-DA), 1,2-dexadecandiol, hexadecylcetylammonium bromide (CTAB), iron(II) chloride [$FeCl_2$], iron(III) pentadianoate [$Fe(acac)_3$], oleic acid, oleylamine, penicillin, sodium diethyldithiocarbamate (DDC), sodium hydroxide, sodium nitroprusside (SNP), fluorescein isothiocyanate (FITC), streptomycin, tetraethyl orthosilicate (TEOS), tri-*n*-octylamine, zinc chloride [$ZnCl_2$], trypsin, and Dulbecco's modified eagle's medium (DMEM) were purchased from Sigma-Aldrich (St. Louis, MO) and used without further purification.

Synthesis of Magnetic Core–Shell Nanoparticles. *Synthesis of Zinc-Doped Magnetic Nanoparticles, MNPs.* The 25 nm $(Zn_{0.4}Fe_{0.6})Fe_2O_4$ magnetic cores were synthesized via modified established procedures published by Cheon et al.[61] Briefly, 1,2-hexadecanediol (10 mmol), $Fe(acac)_3$ (1.35 mmol), $FeCl_2$ (0.7 mmol), and $ZnCl_2$ (0.3 mmol) were added into a 100 mL round-bottom flask with 45.75 mmol of tri-*n*-octylamine and 6 mmol each of oleic acid and oleylamine. Then, under a blanket of nitrogen, the reaction mixture was heated and maintained at 200 °C for 2 h. The mixture was then heated to 300 °C for 2 h. The nanoparticles, thus formed, were then allowed to cool down slowly to room temperature, after which they were collected by centrifugation at 10 000 rpm for 10 min and purified via repeated washing using ethanol.

Synthesis of MNPs and Mesoporous Silica Core–Shell Nanoparticles. To coat the magnetic nanoparticle cores with mesoporous silica, a modified procedure from Kim et al.[62] was used. Alkyl-capped magnetic cores (5 mg) in chloroform were added to a 25 mL solution of 0.1 M aqueous CTAB, followed by sonication via a probe-type sonicator until the formation of a clear solution and evaporation of chloroform. The CTAB-capped magnetic core solution was then diluted to 50 mL, and the pH of this mixture was adjusted to pH 11 using 2 M NaOH. This mixture was heated to 70 °C, and 0.4 mL of TEOS in 2.4 mL of ethyl acetate was added under vigorous stirring. After the addition of TEOS, the reaction was allowed to continue for 4 h. The magnetic mesoporous silica nanoparticles (MSNs) were collected and washed several times with ethanol. To remove the surfactant template, the nanoparticles were heated to 60 °C in an ammonium nitrate solution. The extracted MSNs were again washed with ethanol. The product was confirmed using high-resolution transmission electron microscopy (HR-TEM), dynamic light scattering, and ζ-potential measurement.

APTES Surface Grafting on the MSN. To provide a functional amine group, APTES was grafted onto the MSN surface using a modified method used to graft organosilanes onto silica surfaces.[63] The particles were dried, weighed, and suspended in 15 mL of toluene per 100 mg of MSNs. APTES (40 μL) was then added to the suspension, which was stirred overnight at room temperature.

Formation of THoR-NPs. *iRGD Conjugation on the MSN:* iRGD was conjugated using an established carbodiimide crosslinker chemistry.[64] Briefly, *N*-hydroxy succinimide (2.29 mg) was added to a stirring solution of 1-ethyl-3-(3-dimethylaminopropyl)-carbodiimide hydrochloride (3.1 mg) and iRGD (9.39 mg) in 500 μL of anhydrous dimethylformamide (DMF) at 4 °C. The solution was stirred at this temperature for 30 min and then stirred at room temperature for an additional 4 h, all under an inert atmosphere. Then, APTES-grafted MSN (10 mg) was added dropwise in 500 μL of anhydrous DMF. The mixture was stirred overnight under nitrogen. The nanoparticles were collected by centrifugation and washed several times with methanol and water before being redispersed in PBS at 1 mg/mL.

DDC Loading into THoR-NPs. THoR-NPs (1 mL, 1 mg/mL) were centrifuged at 2000 rpm for 3 min. After the removal of the supernatant, 5 mL of DDC (0.05 g/mL, in PBS) was added and sonicated for 1 min. After 2 h of mixing in the dark, excess DDC was removed by centrifugation (3000 rpm, 3 min). DDC-loaded THoR-NPs were dispersed and sonicated in 1 mL of PBS before use. The amount of entrapped and loaded DDC was evaluated by Ellman's assay.[65] The entrapment efficiency was calculated as

$$\text{entrapment efficiency}(\%) = \frac{\text{DDC}_{\text{total}} - \text{DDC}_{\text{free}}}{\text{DDC}_{\text{total}}} \times 100 \quad (1)$$

The loading efficiency was calculated as

$$\text{loading efficiency}\ (\%) = \frac{\text{mass}_{\text{loaded DDC}}}{\text{mass}_{\text{nanoparticle}}} \times 100 \quad (2)$$

DDC Release Profile of THoR-NPs. DDC-loaded THoR-NPs (1 mL) were incubated under the vigorously stirring condition. The released DDC from the particle was estimated from the supernatant after centrifugation of THoR-NPs. Centrifuged particles were resuspended in 1 mL of pH 7.4 PBS and stirred again. This process was repeated at every collection time point.

Cell Culture. U87-EGFR-viii cells were cultured in DMEM with high glucose (Invitrogen), 10% fetal bovine serum (FBS), 1% streptomycin–penicillin, 1% Glutamax (Invitrogen), and hygromycin B (30 μg/mL), whereas MDA-MB-231 and MCF-7 cells were cultured in DMEM with 10% FBS and 1% streptomycin–penicillin at 37 °C.

Cytotoxicity Assay. To test the sensitivity of U87-EGFR-viii, MDA-MB-231, and MCF-7 cells to DDC and/or SNP compounds, both cells were seeded at a concentration of 20 000 cells/well in 96-well-plates (culture media: DMEM supplemented with 10% FBS, 1% penicillin–streptomycin). After 24 h incubation, serial concentrations of tested compounds were added, and each concentration was tested 4 times. These cells were incubated in a humidified atmosphere with 5% CO_2 for 24 h. Then, 20 μL of 3-(4,5-dimethylthiazol-2-yl)-5-(3-carboxymethoxyphenyl)-2-(4-sulfophenyl)-2*H*-tetrazolium (MTS) solution was added to each well and incubated at 37 °C for 1 h. Fluorescence intensity was measured at 590 with 560 nm excitation using a fluoro-microplate reader (Tecan, Switzerland). The cell viability was determined using the following equation: cell viability = sample's FI × 100/control's FI.

Detection of Intracellular ROS Formation. Reactive species levels were measured using the cell permeable reagent DCFH-DA.[66] Cells were incubated with 100 μM DCFH-DA [dissolved in dimethyl sulfoxide] for 30 min at 37 °C. After incubation, cells were washed with PBS, and the relative levels of fluorescence were quantified using

DOI: 10.1021/acsami.9b07483
ACS Appl. Mater. Interfaces XXXX, XXX, XXX–XXX

a fluoro-microplate reader (excitation: 485 nm and emission: 535 nm).

Analysis of Gene Expression. The messenger RNAs from genes of interest were extracted as total RNA using TRIzol Reagent (Life Technologies, CA) following the standard protocol from the manufacturer. Subsequently, 1 μg of total RNA was primed by oligo(dT) and converted to complementary DNA (cDNA) by Superscript III First-Strand Synthesis System (Life Technologies, CA). The cDNA was subjected to quantitative PCR (qPCR) analysis with the gene-specific primers, listed in Table S1. The qPCR reactions were performed on a StepOnePlus Real-Time PCR System (Applied Biosystems, CA) using Power SYBR Green PCR Master Mix (Applied Biosystems, CA). The fold change in gene expression was calculated based on the resulting *Ct* values of the gene of interest relative to those of endogenous control (GAPDH). Standard cycling conditions were used for all reactions with a melting temperature of 60 °C. All primers were obtained from the PrimerBank database (Table S2).[67−69]

Flow Cytometry. To test the iRGD-mediated target-specific delivery of THoR-NPs, MDA-MB-231, and MCF-7, cells were seeded at a concentration of 100 000 cells/well in 6-well plates. After 24 h incubation, THoR-NPs were treated on both cells with Opti-MEM and incubated for 2 h. The particle solution was washed with PBS and incubated with culture media. Both cells lines were dissociated with trypsin, washed, and resuspended in PBS. Flow cytometry analysis on the samples was performed using a Backman Coulter Gallios Flow Cytometry instrument, and the results were analyzed using the Kaluza software.

Magnetic Hyperthermia. After 24 h of seeding cells, 40 μg/mL of DDC-loaded THoR-NPs were prepared in media and added to each well (24-well plate). After 24 h of transfection, cells were washed with DPBS, trypsinized, and exposed to an alternating magnetic field (5 kA/m, 225 kHz) for the desired amount of time. Thereafter, fresh media were added to the treated cells, and the cells were plated back into 96-well plates.

Generation of Subcutaneous Tumor Xenografts in Mice and Injection of THoR-NPs and SNP. To examine anticancer effects of DDC-loaded THoR-NPs and SNP in the breast cancer tissue, 6-week-old BALB/c nude mice were purchased from RaonBio (Kayonggi-do, Yongin-si, Republic of Korea) (control, n = 4; xenograft, n = 4). All animals were acclimatized to the animal facility for at least 48 h prior to experimentation and maintained according to the Guide for the Care and Use of Laboratory Animals published by the NIH. They were housed in a barrier under HEPA filtration and provided with sterilized food and water ad libitum. The animal facility was maintained under 12 h light/dark cycles at room temperature 21 ± 2 °C with 30−40% humidity. Approximately, 5.0 × 10^6 cells of MDA-MB-231 were mixed with 354234-matrigel (BD, San Jose, CA) and subcutaneously injected in the shoulders and thighs of mice. Studies were conducted when the tumors were ≈4 mm in diameter.

In Vivo SNP Solution and DDC-Loaded Nanoparticle Treatment. For the biodistribution analysis of THoR-NPs, 100 μL (1 mg/mL in PBS) of fluorescein isothiocyanate (FITC)-labeled THoR-NPs were injected intravenously and monitored at different time points (0, 0.5, 1, 2, 4, 6, and 24 h post-injection). To confirm the target-specific delivery of THoR-NPs, major organs included in the circulatory system (heart, liver, kidney, spleen, and lung) and the tumor were extracted from the mouse 24 h post-injection after the euthanasia by CO_2. In vivo imaging system spectrum (PerkinElmer, Waltham, MA) was used to monitor the fluorescence emitted from the FITC-labeled THoR-NPs for in vivo and ex vivo imaging. To validate the nontoxicity of SNP in mice, SNP solutions were treated via iv injection with 24 h interval for 1 week and at different doses: 0.01, 0.1, 1, 10, 25, and 50 mg/(kg min) of SNP in 150 μL PBS. The toxic effect was determined with a survival rate of the mouse. After the selection of the optimum SNP condition, DDC-loaded THoR-NPs were intratumorally injected (1 mg/mL in PBS and 100 μL/site) in tumors of both thighs in the mice. For the control test, PBS was injected into both shoulder's tumor in the same mouse with the same method. To confirm the DDC-loaded THoR-NP's anticancer effects based on synergistic ROS generation in the presence of SNP, particle-injected mice were divided into two groups: group 1, iv injection of SNP solution and group 2, iv injection of PBS as a control. THoR-NPs and SNP solutions were injected at 24 h intervals once a week for 4 weeks, and post-treatment tumor size measurement was measured daily using a caliper before the injection.

Statistical Analyses. All experiments were repeated at least 4 times. Data are shown as means ± standard deviations. Statistical significance was determined by Student's t-test with differences considered statistically significant at a value of $P < 0.05$.

■ ASSOCIATED CONTENT

Supporting Information

The Supporting Information is available free of charge on the ACS Publications website at DOI: 10.1021/acsami.9b07483.

Mechanism of THOR-NP-based synergetic reactive oxygen species (ROS) generation and applications; characterization of magnetic mesoporous silica nanoparticles (MSNs); HR-TEM, DLS, and ζ-potential; in vitro DDC release kinetics of DDC-loaded THoR-NPs in PBS (pH 7.4); synergistic effects of SNP and DDC on malignant breast cancer; effects of cyclopentadiene on cancer cell; time-dependent RS generation of DDC-loaded MSN with magnetic hyperthermia; target-specific delivery of iRGD-functionalized THoR-NPs; ex vivo analysis of THoR-NPs and SNP synergistic therapy; representative H&E staining sections in various organs excised from tumor-bearing mice (magnification: 40×); survival period and rate of SNP injected mouse; table of the primers used for quantitative PCR (PDF)

■ AUTHOR INFORMATION

Corresponding Authors

*E-mail: thkim0512@cau.ac.kr (T.-H.K.).
*E-mail: jwchoi@sogang.ac.kr (J.-W.C.).
*E-mail: kblee@chem.rutgers.edu (K.-B.L.).

ORCID

Hyeon-Yeol Cho: 0000-0003-1897-1166
Thanapat Pongkulapa: 0000-0003-0678-1736
Tae-Hyung Kim: 0000-0003-3671-3830
Jeong-Woo Choi: 0000-0003-0100-0582

Author Contributions

○H.-Y.C. and A.M. contributed equally.

Notes

The authors declare no competing financial interest.

■ ACKNOWLEDGMENTS

J.-W.C. acknowledges financial support from the Basic Science Research Program through the National Research Foundation of Korea (NRF) funded by the Ministry of Education (No.2016R1A6A1A03012845). K.-B.L. acknowledges partial financial support from the NSF (CBET-1803517). A.M. acknowledges financial support from The Scientific and Technological Research Council of Turkey (TUBITAK) (grant number: B.14.2.TBT.0.06.01-219-84).

■ REFERENCES

(1) Xiong, L.; Du, X.; Kleitz, F.; Qiao, S. Z. Cancer-Cell-Specific Nuclear-Targeted Drug Delivery by Dual-Ligand-Modified Mesoporous Silica Nanoparticles. *Small* **2015**, *11*, 5919−5926.

DOI: 10.1021/acsami.9b07483
ACS Appl. Mater. Interfaces XXXX, XXX, XXX−XXX

(2) Zhong, Y.; Meng, F.; Deng, C.; Zhong, Z. Ligand-Directed Active Tumor-Targeting Polymeric Nanoparticles for Cancer Chemotherapy. *Biomacromolecules* **2014**, *15*, 1955−1969.
(3) Cai, X.; Luo, Y.; Zhang, W.; Du, D.; Lin, Y. Ph-Sensitive Zno Quantum Dots-Doxorubicin Nanoparticles for Lung Cancer Targeted Drug Delivery. *ACS Appl. Mater. Interfaces* **2016**, *8*, 22442−22450.
(4) Fan, Z.; Sun, L.; Huang, Y.; Wang, Y.; Zhang, M. Bioinspired Fluorescent Dipeptide Nanoparticles for Targeted Cancer Cell Imaging and Real-Time Monitoring of Drug Release. *Nat. Nanotechnol.* **2016**, *11*, 388−394.
(5) Liu, J.; Wei, T.; Zhao, J.; Huang, Y.; Deng, H.; Kumar, A.; Wang, C.; Liang, Z.; Ma, X.; Liang, X. J. Multifunctional Aptamer-Based Nanoparticles for Targeted Drug Delivery to Circumvent Cancer Resistance. *Biomaterials* **2016**, *91*, 44−56.
(6) Chen, L.; Wu, L.; Liu, F.; Qi, X. Y.; Ge, Y. R.; Shen, S. Azo-Functionalized Fe3o4 Nanoparticles: A near-Infrared Light Triggered Drug Delivery System for Combined Therapy of Cancer with Low Toxicity. *J. Mater. Chem. B* **2016**, *4*, 3660−3669.
(7) Wang, Y.; Strohm, E. M.; Sun, Y.; Wang, Z.; Zheng, Y.; Wang, Z.; Kolios, M. C. Biodegradable Polymeric Nanoparticles Containing Gold Nanoparticles and Paclitaxel for Cancer Imaging and Drug Delivery Using Photoacoustic Methods. *Biomed. Opt. Express* **2016**, *7*, 4125−4138.
(8) Zhu, Y. D.; Chen, S. P.; Zhao, H.; Yang, Y.; Chen, X. Q.; Sun, J.; Fan, H. S.; Zhang, X. D. Ppy@Mil-100 Nanoparticles as a Ph- and near-Ir-Irradiation-Responsive Drug Carrier for Simultaneous Photothermal Therapy and Chemotherapy of Cancer Cells. *ACS Appl. Mater. Interfaces* **2016**, *8*, 34209−34217.
(9) Bairati, I.; Meyer, F.; Gelinas, M.; Fortin, A.; Nabid, A.; Brochet, F.; Mercier, J. P.; Tetu, B.; Harel, F.; Abdous, B.; Vigneault, E.; Vass, S.; Del Vecchio, P.; Roy, J. Randomized Trial of Antioxidant Vitamins to Prevent Acute Adverse Effects of Radiation Therapy in Head and Neck Cancer Patients. *J. Clin. Oncol.* **2005**, *23*, 5805−5813.
(10) Thorn, C. F.; Oshiro, C.; Marsh, S.; Hernandez-Boussard, T.; McLeod, H.; Klein, T. E.; Altman, R. B. Doxorubicin Pathways: Pharmacodynamics and Adverse Effects. *Pharmacogenet. Genomics* **2011**, *21*, 440−446.
(11) Tsuchiya, N.; Inoue, T.; Narita, S.; Kumazawa, T.; Saito, M.; Obara, T.; Tsuruta, H.; Horikawa, Y.; Yuasa, T.; Satoh, S.; Habuchi, T. Drug Related Genetic Polymorphisms Affecting Adverse Reactions to Methotrexate, Vinblastine, Doxorubicin and Cisplatin in Patients with Urothelial Cancer. *J. Urol.* **2008**, *180*, 2389−2395.
(12) Gukovskaya, A. S.; Gukovsky, I. Which Way to Die: The Regulation of Acinar Cell Death in Pancreatitis by Mitochondria, Calcium, and Reactive Oxygen Species. *Gastroenterology* **2011**, *140*, 1876−1880.
(13) Orrenius, S.; Gogvadze, V.; Zhivotovsky, B. Calcium and Mitochondria in the Regulation of Cell Death. *Biochem. Biophys. Res. Commun.* **2015**, *460*, 72−81.
(14) Tong, L.; Chuang, C. C.; Wu, S.; Zuo, L. Reactive Oxygen Species in Redox Cancer Therapy. *Cancer Lett.* **2015**, *367*, 18−25.
(15) Schafer, F. Q.; Buettner, G. R. Redox Environment of the Cell as Viewed through the Redox State of the Glutathione Disulfide/Glutathione Couple. *Free Radical Biol. Med.* **2001**, *30*, 1191−1212.
(16) Bandyopadhyay, U.; Das, D.; Banerjee, R. K. Reactive Oxygen Species: Oxidative Damage and Pathogenesis. *Curr. Sci.* **1999**, *77*, 658−666.
(17) Bergamini, C. M.; Gambetti, S.; Dondi, A.; Cervellati, C. Oxygen, Reactive Oxygen Species and Tissue Damage. *Curr. Pharm. Des.* **2004**, *10*, 1611−1626.
(18) Ishikawa, K.; Takenaga, K.; Akimoto, M.; Koshikawa, N.; Yamaguchi, A.; Imanishi, H.; Nakada, K.; Honma, Y.; Hayashi, J. Ros-Generating Mitochondrial DNA Mutations Can Regulate Tumor Cell Metastasis. *Science* **2008**, *320*, 661−664.
(19) Han, Y. H.; Park, W. H. Tiron, a Ros Scavenger, Protects Human Lung Cancer Calu-6 Cells against Antimycin a-Induced Cell Death. *Oncol. Rep.* **2009**, *21*, 253−261.
(20) He, L.; Chen, T.; You, Y.; Hu, H.; Zheng, W.; Kwong, W. L.; Zou, T.; Che, C. M. A Cancer-Targeted Nanosystem for Delivery of Gold(Iii) Complexes: Enhanced Selectivity and Apoptosis-Inducing Efficacy of a Gold(Iii) Porphyrin Complex. *Angew. Chem., Int. Ed.* **2014**, *53*, 12532−12536.
(21) He, L.; Lai, H.; Chen, T. Dual-Function Nanosystem for Synergetic Cancer Chemo-/Radiotherapy through Ros-Mediated Signaling Pathways. *Biomaterials* **2015**, *51*, 30−42.
(22) Francis, D.; Richards, G. M.; Forouzannia, A.; Mehta, M. P.; Khuntia, D. Motexafin Gadolinium: A Novel Radiosensitizer for Brain Tumors. *Expert Opin. Pharmacother.* **2009**, *10*, 2171−2180.
(23) Yang, R. Y.; Kizer, D.; Wu, H.; Volckova, E.; Miao, X. S.; Ali, S. M.; Tandon, M.; Savage, R. E.; Chan, T. C.; Ashwell, M. A. Synthetic Methods for the Preparation of Arq 501 (Beta-Lapachone) Human Blood Metabolites. *Bioorg. Med. Chem.* **2008**, *16*, 5635−5643.
(24) Kim, Y.-A.; Kim, M.-Y.; Jung, Y.-S. Glutathione Depletion by L-Buthionine-S, R-Sulfoximine Induces Apoptosis of Cardiomyocytes through Activation of Pkc-Δ. *Biomol. Ther.* **2013**, *21*, 358.
(25) Dorr, R. T.; Liddil, J. D.; Klein, M. K.; Hersh, E. M. Preclinical Pharmacokinetics and Antitumor Activity of Imexon. *Invest. New Drugs* **1995**, *13*, 113−116.
(26) Ma, L.; Li, G.; Zhu, H.; Dong, X.; Zhao, D.; Jiang, X.; Li, J.; Qiao, H.; Ni, S.; Sun, X. 2-Methoxyestradiol Synergizes with Sorafenib to Suppress Hepatocellular Carcinoma by Simultaneously Dysregulating Hypoxia-Inducible Factor-1 and -2. *Cancer Lett.* **2014**, *355*, 96−105.
(27) Hao, W.; Yuan, X.; Yu, L.; Gao, C.; Sun, X.; Wang, D.; Zheng, Q. Licochalcone a-Induced Human Gastric Cancer Bgc-823 Cells Apoptosis by Regulating Ros-Mediated Mapks and Pi3k/Akt Signaling Pathways. *Sci. Rep.* **2015**, *5*, No. 10336.
(28) Hou, Z.; Zhang, Y.; Deng, K.; Chen, Y.; Li, X.; Deng, X.; Cheng, Z.; Lian, H.; Li, C.; Lin, J. Uv-Emitting Upconversion-Based Tio2 Photosensitizing Nanoplatform: Near-Infrared Light Mediated in Vivo Photodynamic Therapy Via Mitochondria-Involved Apoptosis Pathway. *ACS Nano* **2015**, *9*, 2584−2599.
(29) Zhang, M.; Harashima, N.; Moritani, T.; Huang, W.; Harada, M. The Roles of Ros and Caspases in Trail-Induced Apoptosis and Necroptosis in Human Pancreatic Cancer Cells. *PLoS One* **2015**, *10*, No. e0127386.
(30) Hu, Y.; Lv, T.; Ma, Y.; Xu, J. J.; Zhang, Y. H.; Hou, Y. L.; Huang, Z. J.; Ding, Y. Nanoscale Coordination Polymers for Synergistic No and Chemodynamic Therapy of Liver Cancer. *Nano Lett.* **2019**, *19*, 2731−2738.
(31) Kim, J.; Kim, H. Y.; Song, S. Y.; Go, S. H.; Sohn, H. S.; Baik, S.; Soh, M.; Kim, K.; Kim, D.; Kim, H. C.; Lee, N.; Kim, B. S.; Hyeon, T. Synergistic Oxygen Generation and Reactive Oxygen Species Scavenging by Manganese Ferrite/Ceria Co-Decorated Nanoparticles for Rheumatoid Arthritis Treatment. *ACS Nano* **2019**, *13*, 3206−3217.
(32) Liu, C.; Wang, D.; Zhang, S.; Cheng, Y.; Yang, F.; Xing, Y.; Xu, T.; Dong, H.; Zhang, X. Biodegradable Biomimic Copper/Manganese Silicate Nanospheres for Chemodynamic/Photodynamic Synergistic Therapy with Simultaneous Glutathione Depletion and Hypoxia Relief. *ACS Nano* **2019**, *13*, 4267−4277.
(33) Wang, S.; Wang, Z.; Yu, G.; Zhou, Z.; Jacobson, O.; Liu, Y.; Ma, Y.; Zhang, F.; Chen, Z. Y.; Chen, X. Tumor-Specific Drug Release and Reactive Oxygen Species Generation for Cancer Chemo/Chemodynamic Combination Therapy. *Adv. Sci.* **2019**, *6*, No. 1801986.
(34) Zhou, Z.; Song, J.; Nie, L.; Chen, X. Reactive Oxygen Species Generating Systems Meeting Challenges of Photodynamic Cancer Therapy. *Chem. Soc. Rev.* **2016**, *45*, 6597−6626.
(35) Poole, K. M.; Nelson, C. E.; Joshi, R. V.; Martin, J. R.; Gupta, M. K.; Haws, S. C.; Kavanaugh, T. E.; Skala, M. C.; Duvall, C. L. Ros-Responsive Microspheres for on Demand Antioxidant Therapy in a Model of Diabetic Peripheral Arterial Disease. *Biomaterials* **2015**, *41*, 166−175.
(36) Wang, L.; Ding, L.; Yu, Z.; Zhang, T.; Ma, S.; Liu, J. Intracellular Ros Scavenging and Antioxidant Enzyme Regulating Capacities of Corn Gluten Meal-Derived Antioxidant Peptides in Hepg2 Cells. *Food Res. Int.* **2016**, *90*, 33−41.

DOI: 10.1021/acsami.9b07483
ACS Appl. Mater. Interfaces XXXX, XXX, XXX−XXX

(37) Huerta, S.; Chilka, S.; Bonavida, B. Nitric Oxide Donors: Novel Cancer Therapeutics (Review). *Int. J. Oncol.* **2008**, *33*, 909−927.
(38) Yang, L.; Lan, C.; Fang, Y.; Zhang, Y.; Wang, J.; Guo, J.; Wan, S.; Yang, S.; Wang, R.; Fang, D. Sodium Nitroprusside (Snp) Sensitizes Human Gastric Cancer Cells to Trail-Induced Apoptosis. *Int. Immunopharmacol.* **2013**, *17*, 383−389.
(39) Ding, W. Q.; Liu, B.; Vaught, J. L.; Yamauchi, H.; Lind, S. E. Anticancer Activity of the Antibiotic Clioquinol. *Cancer Res.* **2005**, *65*, 3389−3395.
(40) Zhou, J.; Zhang, H.; Gu, P.; Bai, J.; Margolick, J. B.; Zhang, Y. Nf-Kappab Pathway Inhibitors Preferentially Inhibit Breast Cancer Stem-Like Cells. *Breast Cancer Res. Treat.* **2008**, *111*, 419−427.
(41) Shah, B. P.; Pasquale, N.; De, G.; Tan, T.; Ma, J.; Lee, K. B. Core-Shell Nanoparticle-Based Peptide Therapeutics and Combined Hyperthermia for Enhanced Cancer Cell Apoptosis. *ACS Nano* **2014**, *8*, 9379−9387.
(42) Sugahara, K. N.; Teesalu, T.; Karmali, P. P.; Kotamraju, V. R.; Agemy, L.; Girard, O. M.; Hanahan, D.; Mattrey, R. F.; Ruoslahti, E. Tissue-Penetrating Delivery of Compounds and Nanoparticles into Tumors. *Cancer Cell* **2009**, *16*, 510−520.
(43) Sugahara, K. N.; Teesalu, T.; Karmali, P. P.; Kotamraju, V. R.; Agemy, L.; Greenwald, D. R.; Ruoslahti, E. Coadministration of a Tumor-Penetrating Peptide Enhances the Efficacy of Cancer Drugs. *Science* **2010**, *328*, 1031−1035.
(44) Murphy, M. P. How Mitochondria Produce Reactive Oxygen Species. *Biochem. J.* **2009**, *417*, 1−13.
(45) Zhao, J.; Zhang, L.; Li, J.; Wu, T.; Wang, M.; Xu, G.; Zhang, F.; Liu, L.; Yang, J.; Sun, S. A Novel Pyrazolone-Based Derivative Induces Apoptosis in Human Esophageal Cells Via Reactive Oxygen Species (Ros) Generation and Caspase-Dependent Mitochondria-Mediated Pathway. *Chem.-Biol. Interact.* **2015**, *231*, 1−9.
(46) Zhou, Y. J.; Zhang, S. P.; Liu, C. W.; Cai, Y. Q. The Protection of Selenium on Ros Mediated-Apoptosis by Mitochondria Dysfunction in Cadmium-Induced Llc-Pk(1) Cells. *Toxicol. In Vitro* **2009**, *23*, 288−294.
(47) Zhu, Z.; Li, R.; Stricker, R.; Reiser, G. Extracellular Alpha-Crystallin Protects Astrocytes from Cell Death through Activation of Mapk, Pi3k/Akt Signaling Pathway and Blockade of Ros Release from Mitochondria. *Brain Res.* **2015**, *1620*, 17−28.
(48) Herrera, E. A.; Krause, B.; Ebensperger, G.; Reyes, R. V.; Casanello, P.; Parra-Cordero, M.; Llanos, A. J. The Placental Pursuit for an Adequate Oxidant Balance between the Mother and the Fetus. *Front. Pharmacol.* **2014**, *5*, No. 149.
(49) Subelzu, N.; Bartesaghi, S.; de Bem, A.; Radi, R. Oxidative Inactivation of Nitric Oxide and Peroxynitrite Formation in the Vasculature. In *Oxidative Stress: Diagnostics, Prevention, and Therapy Volume 2*; ACS Symposium Series; American Chemical Society, 2015; Chapter 4, pp 91−145.
(50) Saxena, A.; Sachin, K.; Bohidar, H. B.; Verma, A. K. Effect of Molecular Weight Heterogeneity on Drug Encapsulation Efficiency of Gelatin Nano-Particles. *Colloids Surf., B* **2005**, *45*, 42−48.
(51) Blaise, G.; To, Q.; Sauve, R. Superoxide-Dismutase (Sod) Can Suppress Halothane Interaction with Nitric-Oxide (No) Stability. *Anesthesiology* **1994**, *81*, A771.
(52) Kast, R. E.; Boockvar, J. A.; Bruning, A.; Cappello, F.; Chang, W. W.; Cvek, B.; Dou, Q. P.; Duenas-Gonzalez, A.; Efferth, T.; Focosi, D.; Ghaffari, S. H.; Karpel-Massler, G.; Ketola, K.; Khoshnevisan, A.; Keizman, D.; Magne, N.; Marosi, C.; McDonald, K.; Munoz, M.; Paranjpe, A.; Pourgholami, M. H.; Sardi, I.; Sella, A.; Srivenugopal, K. S.; Tuccori, M.; Wang, W.; Wirtz, C. R.; Halatsch, M. E. A Conceptually New Treatment Approach for Relapsed Glioblastoma: Coordinated Undermining of Survival Paths with Nine Repurposed Drugs (Cusp9) by the International Initiative for Accelerated Improvement of Glioblastoma Care. *Oncotarget* **2013**, *4*, 502−530.
(53) Baker, A. F.; Landowski, T.; Dorr, R.; Tate, W. R.; Gard, J. M.; Tavenner, B. E.; Dragovich, T.; Coon, A.; Powis, G. The Antitumor Agent Imexon Activates Antioxidant Gene Expression: Evidence for an Oxidative Stress Response. *Clin. Cancer Res.* **2007**, *13*, 3388−3394.
(54) Haam, S. J.; Lee, D. Y.; Paik, H. C. The Effects of Antioxidants (N-Acetylcystein and Epigallocatechin-3-Gallate) in Ischemia-Reperfusion Injury of Rat Lungs. *J. Heart Lung Transplant.* **2009**, *28*, S181.
(55) Chen, C. J.; Deng, A. J.; Liu, C.; Shi, R.; Qin, H. L.; Wang, A. P. Hepatoprotective Activity of Cichorium Endivia L. Extract and Its Chemical Constituents. *Molecules* **2011**, *16*, 9049−9066.
(56) El-Orabi, N. F.; Rogers, C. B.; Edwards, H. G.; Schwartz, D. D. Heat-Induced Inhibition of Superoxide Dismutase and Accumulation of Reactive Oxygen Species Leads to Ht-22 Neuronal Cell Death. *J. Therm. Biol.* **2011**, *36*, 49−56.
(57) Wydra, R. J.; Rychahou, P. G.; Evers, B. M.; Anderson, K. W.; Dziubla, T. D.; Hilt, J. Z. The Role of Ros Generation from Magnetic Nanoparticles in an Alternating Magnetic Field on Cytotoxicity. *Acta Biomater.* **2015**, *25*, 284−290.
(58) Uttara, B.; Singh, A. V.; Zamboni, P.; Mahajan, R. T. Oxidative Stress and Neurodegenerative Diseases: A Review of Upstream and Downstream Antioxidant Therapeutic Options. *Curr. Neuropharmacol.* **2009**, *7*, 65−74.
(59) Floyd, R. A.; Carney, J. M. Free Radical Damage to Protein and DNA: Mechanisms Involved and Relevant Observations on Brain Undergoing Oxidative Stress. *Ann. Neurol.* **1992**, *32*, S22−S27.
(60) Moffett, B. S.; Price, J. F. Evaluation of Sodium Nitroprusside Toxicity in Pediatric Cardiac Surgical Patients. *Ann. Pharmacother.* **2008**, *42*, 1600−1604.
(61) Cheon, J. W.; Seo, J. W.; Lee, J. H. Preparation Method of Magnetic and Metal Oxide Nanoparticles. U.S. Patent US8,066,9692011.
(62) Kim, J.; Kim, H. S.; Lee, N.; Kim, T.; Kim, H.; Yu, T.; Song, I. C.; Moon, W. K.; Hyeon, T. Multifunctional Uniform Nanoparticles Composed of a Magnetite Nanocrystal Core and a Mesoporous Silica Shell for Magnetic Resonance and Fluorescence Imaging and for Drug Delivery. *Angew. Chem., Int. Ed.* **2008**, *47*, 8438−8441.
(63) Kim, J.; Seidler, P.; Fill, C.; Wan, L. S. Investigations of the Effect of Curing Conditions on the Structure and Stability of Amino-Functionalized Organic Films on Silicon Substrates by Fourier Transform Infrared Spectroscopy, Ellipsometry, and Fluorescence Microscopy. *Surf. Sci.* **2008**, *602*, 3323−3330.
(64) Hermanson, G. T. The Reactions of Bioconjugation. In *Bioconjugate Techniques*; Academic Press: Boston, 2013; pp 229−258.
(65) Abu-Serie, M. M. Evaluation of the Selective Toxic Effect of the Charge Switchable Diethyldithiocarbamate-Loaded Nanoparticles between Hepatic Normal and Cancerous Cells. *Sci. Rep.* **2018**, *8*, No. 4617.
(66) Ahn, H. J.; Kim, K. I.; Hoan, N. N.; Kim, C. H.; Moon, E.; Choi, K. S.; Yang, S. S.; Lee, J. S. Targeting Cancer Cells with Reactive Oxygen and Nitrogen Species Generated by Atmospheric-Pressure Air Plasma. *PLoS One* **2014**, *9*, No. e86173.
(67) Wang, X.; Seed, B. A Pcr Primer Bank for Quantitative Gene Expression Analysis. *Nucleic Acids Res.* **2003**, *31*, e154.
(68) Spandidos, A.; Wang, X.; Wang, H.; Dragnev, S.; Thurber, T.; Seed, B. A Comprehensive Collection of Experimentally Validated Primers for Polymerase Chain Reaction Quantitation of Murine Transcript Abundance. *BMC Genomics* **2008**, *9*, 633.
(69) Spandidos, A.; Wang, X.; Wang, H.; Seed, B. Primerbank: A Resource of Human and Mouse Pcr Primer Pairs for Gene Expression Detection and Quantification. *Nucleic Acids Res.* **2010**, *38*, D792−D799.

DOI: 10.1021/acsami.9b07483
ACS Appl. Mater. Interfaces XXXX, XXX, XXX−XXX